FLAME WRINKLING FACTOR DYNAMIC MODELING FOR LARGE EDDY SIMULATIONS OF TURBULENT PREMIXED COMBUSTION

Thomas Schmitt, Matthieu Boileau, Denis Veynante
Laboratoire EM2C
CNRS - Ecole Centrale Paris
Grande Voie des Vignes, 92295, Châtenay-Malabry, France
email: denis.veynante@ecp.fr

Vincent Moureau
CORIA CNRS - INSA et Université de Rouen
Site du Madrillet - BP 8
76801 Saint Etienne du Rouvray, France
email: vincent.moureau@coria.fr

ABSTRACT

Large eddy simulations (LES) of a turbulent jet premixed flame are performed using a dynamic formulation for the flame surface wrinkling factor entering the F-TACLES model. The model parameter is automatically adjusted on the fly, taking advantage of the knowledge of the resolved scales in the flow field. Two cases are considered: a global formulation where the parameter is spatially uniform and depends only on time and a local determination where this parameter varies with both location and time.

The global formulation, in which the model parameter evolves only slightly around its mean value, provides similar results than with a fixed, but adjusted, value. On the other hand, a local parameter is found to increase from low values, corresponding to planar laminar flame fronts, to values larger than in the global case, as the flame is progressively wrinkled by turbulence motions when convected downstream. Moreover, when the flame is submitted to velocity modulations, parameter values, as well as local heat release rates, are clearly related to the large coherent structures developing in the flow, in agreement with previous observations. Then a local dynamic model formulation might play an important role to predict combustion instabilities.

INTRODUCTION

Large eddy simulation (LES), now widely used in turbulent combustion (Pitsch, 2006; Poinsot & Veynante, 2011), gives access to unsteady flame behaviors as encountered during transient ignition (Boileau *et al.*, 2008), combustion instabilities (Menon & Jou, 1991; Roux *et al.*, 2005) or cycle-to-cycle variations in internal combustion engines (Richard *et al.*, 2007). The unresolved flame / turbulence interactions may be described in terms of sub-grid scale turbulent flame speed (Pitsch, 2006), flame surface density (Boger *et al.*, 1998) or flame surface wrinkling factor (Colin *et al.*, 2000; Charlette *et al.*, 2002*a*). Models generally retain algebraic expressions assuming an equilibrium between turbulence motions and flame surface. However, this assumption fails, for example, in the stabilization region of jet flames or during the transient development following the ignition of a flame kernel: the flame front is initially laminar and is progressively wrinkled by the ambient turbulence. To handle these situations, a refined approach is to solve an additional balance equation for the flame surface density (Hawkes & Cant, 2000; Richard *et al.*, 2007) or the flame wrinkling factor (Weller *et al.*, 1998).

A promising alternative is to automatically adjust algebraic model parameters during the simulation from the known resolved flow field. However, while this approach is now routinely used for unresolved transport since the pioneering work of Germano *et al.* (1991), relatively few works attempt to develop dynamic combustion models (Charlette *et al.*, 2002*b*; Pitsch, 2006; Knudsen & Pitsch, 2008; Wang *et al.*, 2011, 2012; Hawkes *et al.*, 2012). The formulation and the practical implementation of flame wrinkling factor dynamic models is investigated here. The wrinkling factor describes interactions between flame fronts and turbulence motions and enters Level-Set (Pitsch, 2006; Knudsen & Pitsch, 2008), Thickened Flame (Colin *et al.*, 2000; Charlette *et al.*, 2002*a*), algebraic flame surface density (Boger *et al.*, 1998) or F-TACLES (Fiorina *et al.*, 2009) models. The proposed approach is implemented in an LES solver and results are validated against experimental data from a turbulent jet flame (Chen *et al.*, 1996).

MODELING

The filtered reaction rate is written under the generic form (Charlette *et al.*, 2002*a*; Veynante *et al.*, 2012):

$$\overline{\dot{\omega}(c)} = \Xi_\Delta W_\Delta(\widetilde{c}, \Delta) \tag{1}$$

where the progress variable c stands for any quantity entering the reaction rate. $W_\Delta(\widetilde{c}, \Delta)$ is the resolved reaction rate, estimated from mass-weighted filtered quantities $(\widetilde{c})$ and Δ, the LES filter size. The wrinkling factor Ξ_Δ measures the ratio of total to resolved flame surfaces in the filtering volume

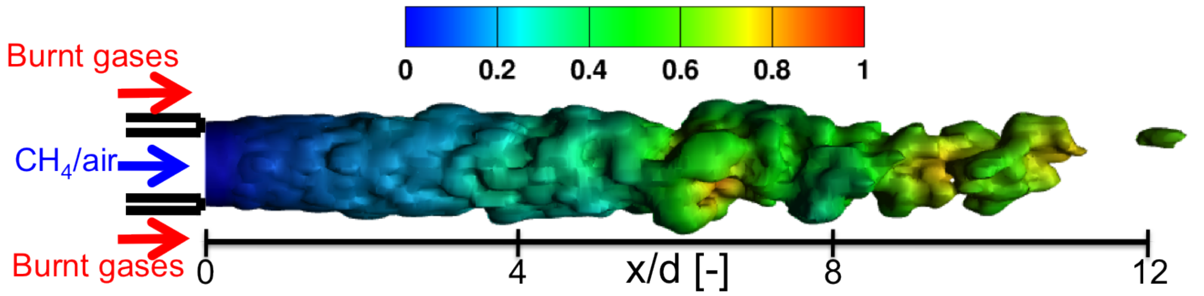

Figure 1. Instantaneous field of the $\widetilde{c} = 0.7$ iso-surface of the filtered progress variable colored by the model parameter value β in the LES of the Chen *et al.* (1996) jet flame (Case F3, inlet jet velocity 30 m s^{-1}, stoichiometric conditions).

(flamelet assumption). It may be modeled by the algebraic expression (Charlette *et al.*, 2002*a*; Wang *et al.*, 2012):

$$\Xi_\Delta = \left(1+\min\left[\max\left(\frac{\Delta}{\delta_c}-1,0\right),\Gamma\left(\frac{\Delta}{\delta_l},\frac{u'_\Delta}{S_l},Re_\Delta\right)\frac{u'_\Delta}{S_l}\right]\right)^\beta \qquad (2)$$

The efficiency function Γ measures the ability of vortices to effectively wrinkle the flame front, u'_Δ and $Re_\Delta = u'_\Delta \Delta/\nu$ are the sub-grid scale turbulence intensity and Reynolds number, respectively, ν being the fresh gas kinematic viscosity. δ_l and S_l are the laminar flame thickness and speed, respectively, while δ_c, the flame cut-off length scale, measures the smallest flame wrinkling length scale. β is the model parameter to be specified. Practical implementation as well as direct numerical simulations (Veynante *et al.*, 2012) show that Eq. (2) is often saturated (i.e. minimum term related to Δ/δ_c and independent of u'_Δ) and reduces to:

$$\Xi_\Delta = \left(\frac{\Delta}{\delta_c}\right)^\beta \qquad (3)$$

where $D = \beta + 2$ is the fractal dimension of the flame surface (Gouldin, 1987). The parameter β is dynamically determined by equating the reaction rate averaged over a given volume ($< \cdot >$), when evaluated at the LES-filter (Δ) and test-filter ($\widehat{\Delta}$) scales:

$$\left\langle \widehat{\left(\frac{\Delta}{\delta_c}\right)^\beta W_\Delta\left(\widetilde{c},\Delta\right)} \right\rangle = \left\langle \left(\frac{\gamma\Delta}{\delta_c}\right)^\beta W_{\gamma\Delta}\left(\widetilde{\widetilde{c}},\gamma\Delta\right)\right\rangle \qquad (4)$$

where $\widetilde{\widetilde{c}}$ denotes a mass-weighted filtering at scale $\widehat{\Delta}$ of the filtered progress variable $\widetilde{c}$. $\gamma\Delta = (\Delta^2 + \widehat{\Delta}^2)^{1/2}$ is the effective filter size when combining LES and test Gaussian filters. Equation (4) then provides a relation to evaluate β. Two key requirements are considered here: *(i)* to recover unity wrinkling factors ($\Xi_\Delta = 1$ and $\beta = 0$), when the flame wrinkling is fully resolved in simulations; *(ii)* to replace the averaging operation $< . >$ by a Gaussian filter, easier to implement for unstructured meshes and/or on massively parallel machines (diffusion operation). The best solution found is to recast Eq. (4) in terms of flame surfaces:

$$\left\langle \widehat{\left(\frac{\Delta}{\delta_c}\right)^\beta |\nabla\overline{c}|} \right\rangle = \left\langle \left(\frac{\gamma\Delta}{\delta_c}\right)^\beta \left|\nabla\widehat{\overline{c}}\right| \right\rangle \qquad (5)$$

where $|\nabla\overline{c}|$, $\Xi_\Delta|\nabla\overline{c}|$, $|\nabla\widehat{\overline{c}}|$ and $\Xi_{\gamma\Delta}|\nabla\widehat{\overline{c}}|$ measure resolved and total flame surface densities at LES and test-filter scales, respectively. Unfortunately, Eq. (5) involves filtered quantities instead of Favre-filtered quantities that are solved for in LES. However, for infinitely thin flame fronts, $\overline{\rho}\widetilde{c} = \overline{\rho c} = \rho_b\overline{c}$ and $\widehat{\overline{\rho}}\widetilde{\widetilde{c}} = \widehat{\overline{\rho c}} = \rho_b\widehat{\overline{c}}$, where ρ_b is the burnt gas density. These relations suggest to approximate β, assumed to be uniform over the averaging volume, as:

$$\beta \approx \frac{\ln\left(\left\langle \widehat{|\nabla\overline{\rho c}|}\right\rangle / \left\langle \left|\nabla\widehat{\overline{\rho}}\widetilde{\widetilde{c}}\right|\right\rangle\right)}{\ln(\gamma)} \approx \frac{\ln\left(\left\langle \widehat{|\nabla\overline{c}|}\right\rangle / \left\langle \left|\nabla\widehat{\overline{c}}\right|\right\rangle\right)}{\ln(\gamma)} \qquad (6)$$

which is well-sustained by direct numerical simulations (Veynante *et al.*, 2012).

NUMERICAL SIMULATIONS

This formalism is implemented in the structured low-Mach code FASTEST from TU-Darmstadt (Germany) to perform LES of the Chen *et al.* (1996) premixed methane / air F3 jet stoichiometric flame, stabilised by a coflow of burnt gases. The dynamic procedure is combined with F-TACLES (Schmitt *et al.*, 2013), where the resolved reaction rate $W_\Delta(\widetilde{c},\Delta)$ in Eq. (1) is estimated from filtered one-dimensional laminar premixed flames (Fiorina *et al.*, 2009).

The mesh contains 800 000 hexahedra and grid spacing is kept constant over the region of interest (Δ_x=0.6 mm, while the injector diameter is d=12 mm). A pipe of 60d length upstream of the injector is included in the computation domain to reach a fully developed turbulent flow at the burner inlet. The filter and test-filter sizes are $\Delta = 3$ mm and $\widehat{\Delta} = 1.5\Delta$, respectively. The flame wrinkling cut-off scale δ_c is set to two times the thermal flame thickness $\delta_l = 0.6$ mm as evaluated from the maximum progress variable gradient, in agreement with Knikker *et al.* (2002). Statistics are extracted averaging simulations over 5 convective times τ_c ($\tau_c = L_{fl}/u_0 = 5$ ms, where $L_{fl} \approx 0.15$ m is the flame length and $u_0 = 30$ m/s the inlet bulk velocity).

The first investigated case considers steady state operating conditions and is devoted to the validation of the dynamic procedure against the available experimental data. In the second case, the incoming jet velocity is modulated to mimic the flow pulsation that could be induced by combustion instabilities and analyze the model response to strong unsteady motions. In each case, the averaging domain $\langle\cdot\rangle$ in Eq. (6) is set to the entire computational domain, leading to the determination of a global model parameter evolving only with time, or to a small volume, corresponding to a Gaussian filter of size $\Delta_m = 2.5\widehat{\Delta}$. ("local" parameter).

Steady-state operating conditions

Figure 1 displays a snapshot of the turbulent jet flame where a progress variable iso-surface is colored by the local model parameter value. As expected, β is small in the initial flame region and increases downstream, as the flame is progressively wrinkled by turbulence motions. Large values are observed in the flame tip. This evolution is confirmed by Fig. 2 displaying the downstream evolution of the mean β value. Note that the β-rms remain low, excepted in pockets detaching at the tip of the main flame. On the other hand, a global model parameter oscillates around a mean value of about $\beta_m = 0.3$ (Fig. 3). In this last case, similar results would be achieved setting $\beta = 0.3$ without dynamic formulation. However, Wang *et al.* (2011) showed that this optimal value depends on the operating conditions.

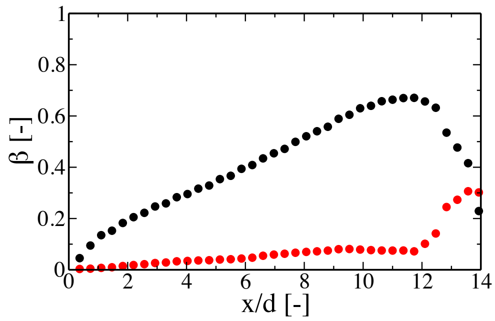

Figure 2. Downstream evolution of the conditional (for 0.6< $\tilde{c}$ <0.8) average (black) and rms (red) of the model parameter β in the F3 Chen *et al.* (1996) jet flame. Downstream coordinate x is made non-dimensional by the jet diameter d=12 mm. Averaging is performed over $4\tau_c$.

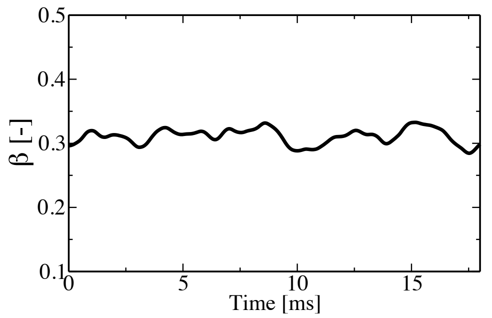

Figure 3. Time evolution of the global model parameter.

Figure 4 compares snapshots of the instantaneous reaction rate for global and local model model parameters. The flames behave differently: when using a local parameter, the flame is less (respectively more) intense in the initial (final) region when compared to the global parameter case. This finding is in agreement with Figs. 2 and 3: the local model parameter, and accordingly the flame wrinkling factor Ξ_Δ and the progress variable reaction rate, is lower than the mean value $\beta_m = 0.3$ during the initial development of the flame brush. On the other hand, β becomes larger than β_m further downstream, predicting larger wrinkling factors and reaction rates. These results are confirmed by the mean reaction rate fields displayed in Fig. 5.

Mean methane (Y_{CH_4}) and carbon dioxide (Y_{CO_2}) mass fraction transverse profiles are compared to experimental values by Chen *et al.* (1996) for several downstream locations in Fig. 6. Three cases are considered: global and local model parameters together with the assumption that the flame is fully resolved in the simulation ($\Xi_\Delta = 1$). The corresponding rms are presented in Fig. 7. Profiles are very similar for the two first locations ($x/d = 2.5$ and 4.5) while the influence of the sub-grid model is clearly visible for $x/d \geq 6.5$ where the assumption $\Xi_\Delta = 1$ leads to underestimate CO_2 mass fractions and reaction rates. The overall agreement with experimental data is very good, noting that the local dynamic formalism, predicting larger reaction rate values at the flame tip, provides better results for $x/d = 8.5$. Moreover, the flame dynamics is affected by the combustion model: the local model predicts higher rms for locations $x/d \geq 6.5$, in the region where flame fronts interact (see Figs. 4 and 5). The unsteady behavior of the flame is now investigated pulsating the inlet flow velocity.

Pulsating inlet flow

The inlet jet mean velocity is now modulated at a frequency $f_e = 1000$ Hz according to:

$$u = u_0\left(1 + 0.2\sin\left(2\pi f_e t\right)\right) \tag{7}$$

Figure 8 compares four phase averaged filtered progress variable reaction rate fields as predicted using global and local model parameters. The development of the large coherent structures induced by the flow modulation is similar in both cases but the amplitude of the reaction rate variations is larger with local parameter where maximum reaction rate values are located in the highly wrinkled regions of the vortices. Also, as reaction rates are larger at the flame tip in this last case, smaller pockets detach from the main flame and the flame length is slightly reduced. These results are complemented by Fig. 9 where the local model parameter field is superimposed to three iso-surfaces of the phase averaged filtered progress variable corresponding to the reaction zone for the same phases of the pulsating cycle. The model parameter, and then the wrinkling factor Ξ_Δ (Eq. 3), is clearly larger in the highly wrinkled regions of the vortices induced by the flow modulation, in qualitative agreement with previous experimental findings by Nottin *et al.* (2000). Accordingly, the local model parameter has a strong influence on the unsteady heat release rate and may then play a role in the prediction of the dynamical behavior of the flame, especially when combustion instabilities occur. This point is confirmed by Fig. 10 displaying the evolution of the total reaction rate in the computational volume with time: to use a local model parameter leads to a larger, and slightly shifted in phase, flame response to the modulation, compared to the global model parameter. However, this analysis needs to be refined in a near future.

CONCLUSIONS

A dynamic formulation for the flame surface wrinkling factor, automatically adjusting the model parameter during the simulations, has been combined with the F-TACLES model to performed large eddy simulations of a turbulent jet flame. To retain a spatially uniform parameter provides similar results than a non-dynamic formulation. On the other hand, local parameters increase from low values close to

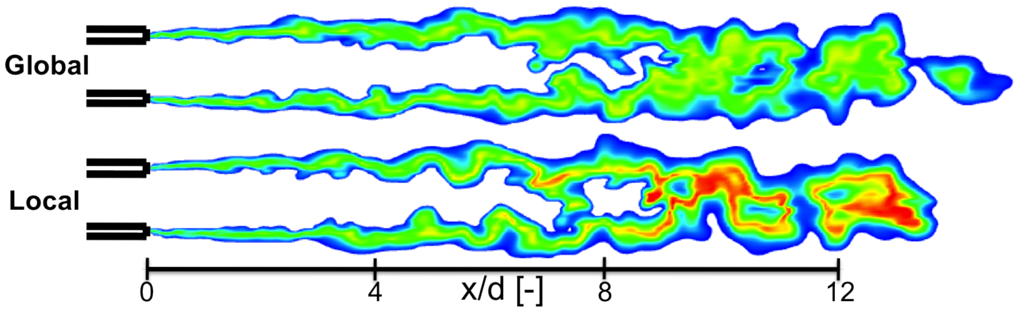

Figure 4. Instantaneous snapshots of the filtered progress variable reaction rate $\overline{\dot{\omega}}(c)$ when considering a global (top, Fig. 3) and a local (bottom, Fig. 2) model parameter. The red color denotes the maximum reaction rate, observed when using a local model parameter, while blue corresponds to 5 % of this maximum value.

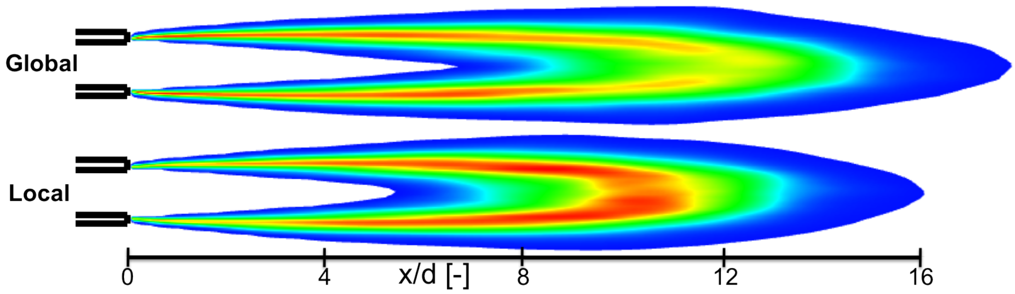

Figure 5. Mean progress variable reaction rate fields as extracted from global (top) and local (bottom) parameter simulations. The red color denotes the maximum reaction rate, while blue corresponds to 5 % of this maximum value.

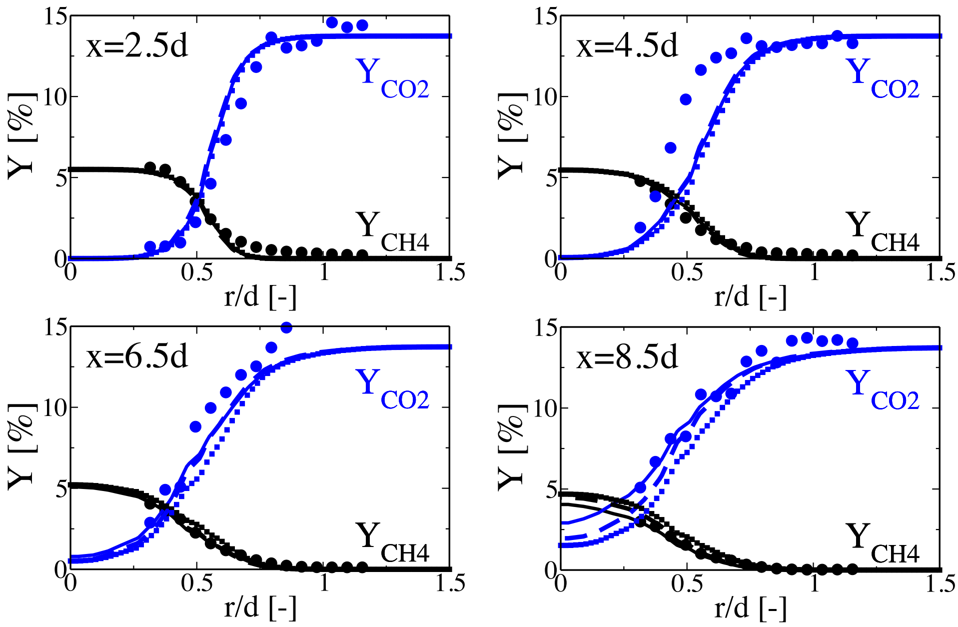

Figure 6. Transverse profiles of mean filtered methane $\widetilde{Y}_{CH_4}$ and carbon dioxide $\widetilde{Y}_{CO_2}$ mass fractions for four downstream locations x/d in the Chen *et al.* (1996) turbulent jet flame (case F3). Line: local model; dashed line: global model; squares: no sub-grid scale model ($\Xi_\Delta = 1$); circles: experiments. Averaging over $5\tau_c$ where τ_c is the convective time.

the injector lips, where the flame is quasi laminar, to large values as the flame is progressively wrinkled by turbulence motions when convected downstream.

The model sensitivity to strong unsteady motions as encountered in combustion instabilities is then analyzed by modulating the inlet flow velocity. Parameter values, and accordingly local heat release rates, are clearly related to the large flow coherent structures, in agreement with previous observations. Such a model formulation might then play a key role in the prediction of instabilities, a point to be investigated in the future.

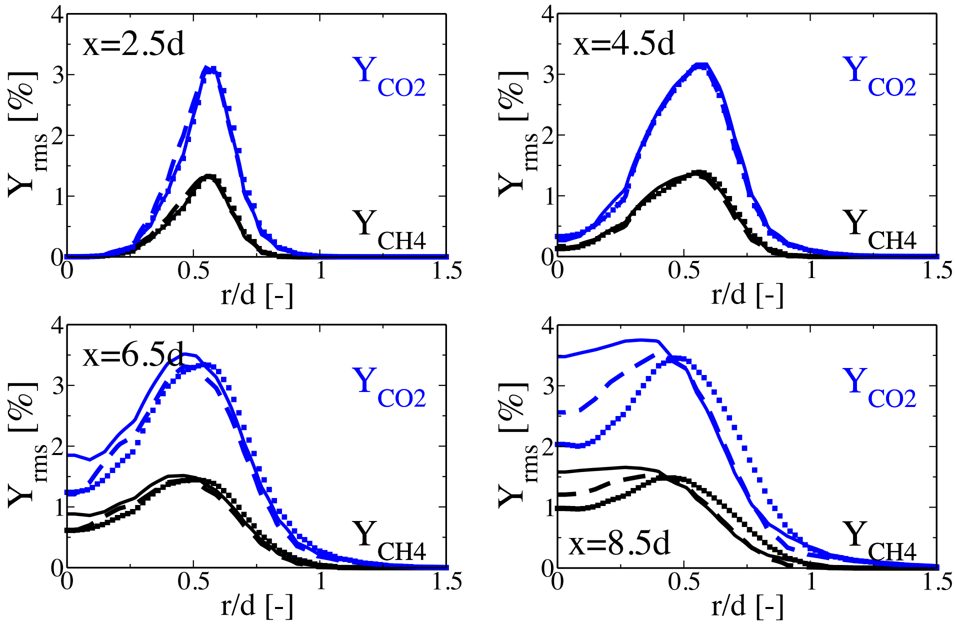

Figure 7. Transverse profiles of rms of filtered methane $\widetilde{Y}_{CH_4}$ and carbon dioxide $\widetilde{Y}_{CO_2}$ mass fractions for four downstream locations x/d in the Chen *et al.* (1996) turbulent jet flame (case F3). Line: local model; dashed line: global model; squares: no sub-grid scale model ($\Xi_\Delta = 1$). Averaging over $5\tau_c$.

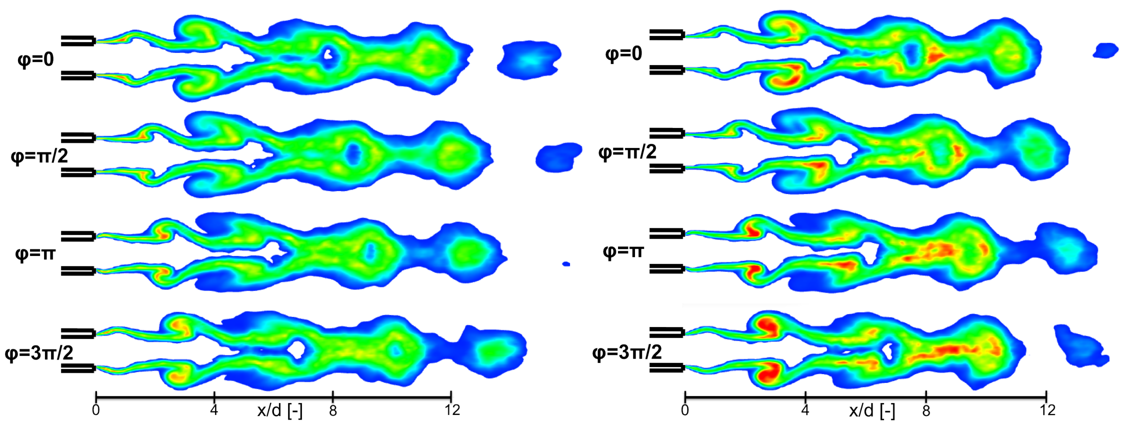

Figure 8. Phase averaged filtered progress variable reaction rate fields when using global (left) and local (right) model parameters for four phases of the pulsation cycle (from top to bottom).

ACKNOWLEDGMENT

The authors warmly acknowledge the support of the Center for Turbulence Research (CTR) at Stanford University (USA) during the 2012 Summer Program, as well as the EKT laboratory (TU-Darmstadt, Germany) for making the FASTEST code available.

REFERENCES

Boger, M., Veynante, D., Boughanem, H. & Trouvé, A. 1998 Direct numerical simulation analysis of flame surface density concept for large eddy simulation of turbulent premixed combustion. *Proc. Combust. Inst.* **27**, 917 – 925.

Boileau, M., Staffelbach, G., Cuenot, B., Poinsot, T. & Bérat, C. 2008 LES of an ignition sequence in a gas turbine engine. *Combust. Flame* **154** (1-2), 2 – 22.

Charlette, F, Meneveau, C. & Veynante, D. 2002*a* A power-law flame wrinkling model for LES of premixed turbulent combustion. Part I: Non-dynamic formulation and initial tests. *Combust. Flame* **131** (1/2), 159 – 180.

Charlette, F, Meneveau, C. & Veynante, D. 2002*b* A power-law flame wrinkling model for LES of premixed turbulent combustion. Part II: Dynamic formulation. *Combust. Flame* **131** (1/2), 181 – 197.

Chen, Y.C., Peters, N., Schneemann, G.A., Wruck, N., Renz, U & Mansour, M.S. 1996 The detailed flame structure of hightly stretched turbulent premixed methane-air flame. *Combust. Flame* **107**, 223 – 244.

Colin, O., Ducros, F., Veynante, D. & Poinsot, T. 2000 A thickened flame model for large eddy simulations of turbulent premixed combustion. *Phys. Fluids A* **12** (7), 1843 – 1863.

Fiorina, B., Gicquel, O. & Veynante, D. 2009 Turbulent flame simulation taking advantage of tabulated chemistry self-similar properties. *Proc. Comb. Institute* **32** (2), 1687–1694.

Germano, M., Piomelli, U., Moin, P. & Cabot, W.H. 1991 A

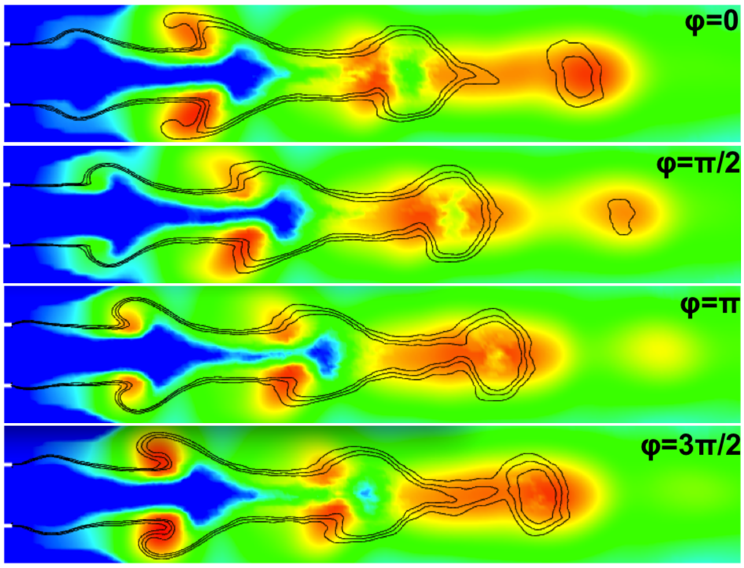

Figure 9. Phase averaged model parameter fields (blue: $\beta = 0$; red: $\beta = 0.8$) superimposed to three filtered progress variable iso-surfaces (lines, $\widetilde{c} = 0.6$; 0.7 and 0.8, maximum reaction rate corresponding to $\widetilde{c} \approx 0.7$). Same instants than Fig. 8.

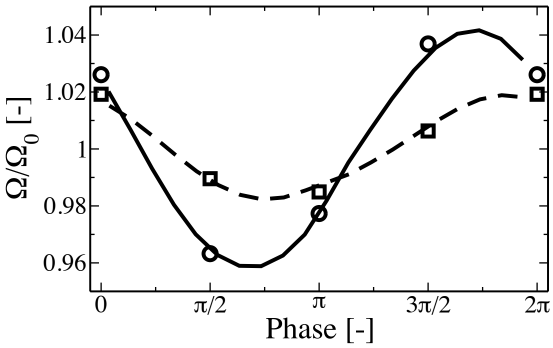

Figure 10. Evolution of the phase averaged total progress variable reaction rate over the computational domain, Ω, reduced by the total mean reaction rate Ω_0, as a function of the pulsation phase for global (dashed line) and local (solid line) formalisms. Symbols correspond to phases displayed in Figs 8 and 9. Phase averaging over 25 cycles and $5\tau_c$.

dynamic subgrid-scale eddy viscosity model. *Phys. Fluids A* **3** (7), 1760 – 1765.

Gouldin, F.C. 1987 An application of fractals to modeling premixed turbulent flames. *Combust. Flame* **68** (3), 249 – 266.

Hawkes, E.R. & Cant, S.R. 2000 A flame surface density approach to large eddy simulation of premixed turbulent combustion. *Proc. Combust. Inst.* **28**, 51 – 58.

Hawkes, E.R., Chatakonda, O., Kolla, H., Kerstein, A.R. & Chen, J.H. 2012 A petascale direct numerical simulation study of the modelling of flame wrinkling for large-eddy simulations in intense turbulence. *Combust. Flame* **159** (8), 2690 – 2703.

Knikker, R., Veynante, D. & Meneveau, C. 2002 A priori testing of a similarity model for large eddy simulations of turbulent premixed combustion. *Proc. Combust. Inst.* **29**, 2105 – 2111.

Knudsen, E. & Pitsch, H. 2008 A dynamic model for the turbulent burning velocity for large eddy simulation of premixed combustion. *Combust. Flame* **154**, 740 – 760.

Menon, S. & Jou, W.H. 1991 Large eddy simulations of combustion instability in an axisymmetric ramjet combustor. *Combust. Sci. Technol.* **75** (1-3), 53 – 72.

Nottin, C., Knikker, R., Boger, M. & Veynante, D. 2000 Large eddy simulations of an acoustically excited turbulent premixed flame. *Proc. Comb. Institute* **28**, 67 – 73.

Pitsch, H. 2006 Large-eddy simulation of turbulent combustion. *Annu. Rev. Fluid Mech.* **38**, 453 – 482.

Poinsot, T. & Veynante, D. 2011 *Theoretical and Numerical Combustion*, 3rd edn.

Richard, S., Colin, O., Vermorel, O., Benkenida, A., Angelberger, C. & Veynante, D. 2007 Towards large eddy simulation of combustion in spark ignition engines. *Proc. Combust. Inst.* **31** (2), 3059 – 3066.

Roux, S., Lartigue, G., Poinsot, T., Meier, U. & Bérat, C. 2005 Studies of mean and unsteady flow in a swirled combustor using experiments, acoustic analysis and large eddy simulations. *Combust. Flame* **141** (1-2), 40 – 54.

Schmitt, T., Sadiki, A., Fiorina, B. & Veynante, D. 2013 Impact of dynamic wrinkling model on the prediction accuracy using the F-TACLES combustion model in swirling premixed turbulent flames. *Proceedings of the Combustion Institute* **34** (1), 1261–1268.

Veynante, D., Schmitt, T., Boileau, M. & Moureau, V. 2012 Analysis of dynamic models for turbulent premixed combustion. In *Proceedings of the Summer Program*. Center for Turbulence Research, NASA Ames/Stanford Univ.

Wang, G., Boileau, M. & Veynante, D. 2011 Implementation of a dynamic thickened flame model for large eddy simulations of turbulent premixed combustion. *Combust. Flame* **158** (11), 2199–2213.

Wang, G., Boileau, M., Veynante, D. & Truffin, K. 2012 Large eddy simulation of a growing turbulent premixed flame kernel using a dynamic flame surface density model. *Combust. Flame* **159** (8), 2742 – 2754.

Weller, H.G., Tabor, G., Gosman, A.D. & Fureby, C. 1998 Application of a flame-wrinkling LES combustion model to a turbulent mixing layer. *Proc. Combust. Inst.* **27**, 899 – 907.